

Diffusive coupling facilitates and impedes noise-induced escape in interacting bistable elements

Hidemasa Ishii^{1,*} and Hiroshi Kori¹

¹Department of Complexity Science and Engineering, Graduate School of Frontier Sciences, the University of Tokyo, Chiba 277-8561, Japan

*hidemasaishii1997@g.ecc.u-tokyo.ac.jp

ABSTRACT

Diverse complex systems often undergo sudden changes in their states, such as epileptic seizures, climate changes, and social uprisings. Such behavior has been modeled by noise-induced escape of bistable elements, which is the escape from an attracting state driven by a fluctuation in the system's state. We consider a system of interacting bistable elements and investigate the effect of diffusive coupling among elements on the process of noise-induced escape. We focus on the influence of the coupling strength over the escape time, which is the time it takes for noise-induced escape to occur. We performed numerical simulations and observed that weak coupling reduced the mean escape time, whereas strong coupling impeded escape. We argue that, although diffusive coupling both facilitates and impedes escape, the facilitating effect is dominant when coupling is weak. For weak coupling cases, we develop an approximate theory that can predict the mean and variance of escape times. In contrast, strong coupling reduces the effective noise intensity to impede escape. Our results suggest that diffusive coupling among multistable elements contributes to regulating the rate of transitions among attracting states.

Introduction

Epileptic brains¹, ecosystems², and firms adopting innovations³ — such diverse complex systems exhibit the similar behavior, wherein their states undergo abrupt changes among multiple stable states. This phenomenon has attracted much attention under the terms such as “tipping points”, “thresholds and breakpoints”, and “regime shifts”⁴. Bistable models, where a system has two distinct attracting states, play an essential role in studying such sudden transitions among different states. Since complex systems often consist of a number of components that interact with each other, models of interacting bistable elements have been studied in diverse contexts, including epilepsy^{5,6}, abrupt change in ecosystems⁷, climate change⁸, poverty traps⁹, and the spread of uprising during the Arab Spring¹⁰. A pile of theoretical literature also exist, for instance on the influence of underlying network structures¹¹ and the prediction of tipping points^{12–14}.

When a bistable system is deterministic, its two attracting states are also stationary states. Hence, the system converges into one of the two states [figure 1(b)]. In deterministic cases, the interaction with other bistable elements causes the propagation of one stationary state and also the coexistence of the two stationary states among elements^{15–18}. The propagation and coexistence have been observed empirically in mechanical systems^{19,20} and electrochemical reactions^{21,22}. When a bistable system is stochastic, its state not only fluctuates about an attracting state but also transitions between the two attracting states intermittently [figure 1(c)]. Because the escape from an attracting state is driven by noise, it is called noise-induced escape. In stochastic cases, the interaction among bistable elements affects the rate of noise-induced escape^{5,23–26}.

A transition among attracting states corresponds to a dramatic change in the system's state, such as an epileptic seizure, extinction of a species, and a riot. Therefore the mean escape time, which is the time it takes for noise-induced escape to occur, is of particular interest. Among the literature on systems of coupled stochastic bistable elements, Frankowicz and Gudowska-Nowak²³ reported in 1982 that, while weak diffusive coupling reduced the mean escape time, stronger coupling slowed down escape. Recently, Creaser and the colleagues²⁶ also briefly referred to this non-monotonic dependence of the mean escape time on the coupling strength. Previous research has mainly studied small systems with 2 or 3 elements, as they are analytically tractable and computationally less demanding. Considering that many real systems — such as brains, ecosystems, and society — consist of a number of components, the effect of the coupling strength on the mean escape time need be investigated for larger systems as well. For small systems, several studies^{25,26} succeeded in estimating the mean escape time utilizing the multidimensional Kramers' formula. However, a similar analytical approach deems infeasible for larger systems due to their large degrees of freedom. Moreover, even though the formula mathematically explains the relation between the coupling strength and the mean escape time, we still lack an intuitive understanding on the influence of the interaction among bistable elements over the process of noise-induced escape.

In this research, we consider a larger system of interacting bistable elements. We assume diffusive coupling among elements,

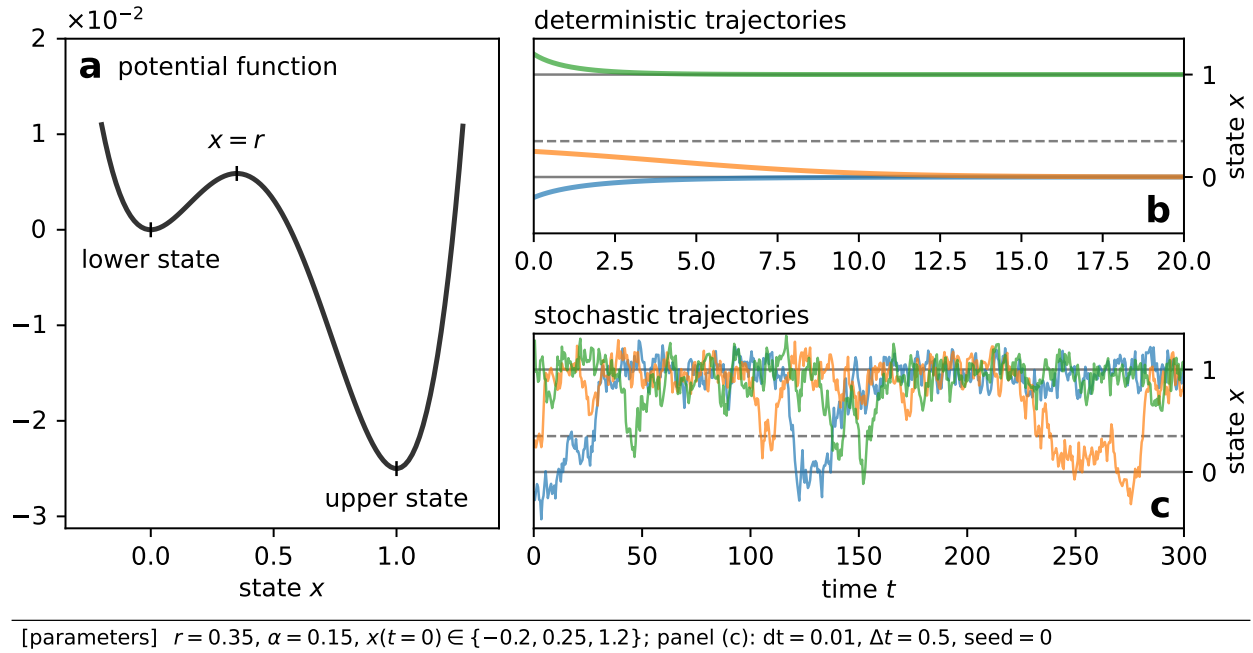


Figure 1. While a state of a deterministic bistable element converges to an attracting state, noise-induced escape from an attracting state occurs when the system is subjected to noise. (a) Illustration of a bistable potential [equation (3)] for $r < 1/2$. (b) Trajectories of an isolated deterministic bistable element, $dx/dt = f(x)$, with three initial conditions. (c) Trajectories of an isolated stochastic bistable element [equation (1)] with three initial conditions.

i.e. each element is affected by the difference between its state and others' states. Diffusive coupling has been assumed in the literature on noise-induced escape in systems of interacting bistable elements^{23,25,26}, and on pattern formation in networked bistable reaction-diffusion models^{15–18,21,22}. In addition, it has been employed to model mechanical systems^{19,20}, epileptic brain⁵, and ecosystem⁷.

Our first result is the relation between the coupling strength and the numerically measured mean escape time. Direct numerical simulations revealed that weak coupling accelerates escape on average, while strong coupling impedes escape. We then discuss the role of diffusive coupling in the process of noise-induced escape. As mentioned above, an analytical approach similar to the previous studies is infeasible. Instead, we describe how weak and strong coupling would change the behavior of each bistable element. Whereas diffusive coupling to a node that has already escaped facilitates escape, interaction with a node that has not escaped impedes escape. When coupling is weak, the balance between these facilitating and impeding effects determines the mean escape time. For weak coupling cases, we develop an approximate theory that predicts the mean and variance of escape times. As coupling becomes stronger, the effective noise intensity for the system declines. We discuss the scaling of the effective noise intensity for strong coupling cases. To facilitate analyses, our model assumes the global coupling among elements and the asymmetric bistability, where the stabilities of the two attracting states differ. Still, we expect that coupling affects the process of noise-induced escape in a qualitatively similar manner on other network structures or with the symmetric bistability. This research thus offers fundamental insights into the role of diffusive coupling in systems of interacting multistable elements, which have been employed in diverse fields from biology to social sciences.

Model

Dynamics of each element

First, we introduce the basic model that describes the dynamics of each element. When we assume no interaction among elements, our model reduces to the following stochastic differential equation (SDE),

$$dx = f(x) dt + \alpha dW(t), \tag{1}$$

where

$$f(x) := -x(x-r)(x-1), \tag{2}$$

x denotes the state of one element, α is the noise intensity, and $W(t)$ is a standard Wiener process. $f(x)$, which was introduced by Schlögl²⁷, describes the deterministic bistable dynamics of each element. Its double-well potential

$$V(x) := \frac{1}{4}x^4 - \frac{1+r}{3}x^3 + \frac{r}{2}x^2, \quad (3)$$

which satisfies $f(x) = -dV(x)/dx$, is plotted in figure 1(a). The deterministic dynamics $\dot{x} = f(x)$ has two attracting states located at the two minima of $V(x)$. The lower attracting state is at $x = 0$, and the upper one is at $x = 1$. Parameter $r \in (0, 1)$ controls the asymmetry of the potential. That is, the relative stability of the upper state against the lower one increases as r gets smaller. We assume r is small, in which case the transition from the upper to lower state is rare enough to be negligible.

Globally coupled stochastic bistable elements

In this paper, we consider a globally coupled network whose each node is the stochastic bistable element. The dynamics of the system is governed by the following SDE,

$$dx_i = \left[f(x_i) + \frac{K}{N} \sum_{j=1}^N (x_j - x_i) \right] dt + \alpha dW_i(t), \quad (4)$$

where x_i denotes the state of node i , K is the coupling strength, N is the number of nodes in a system, and $W_i(t)$ are independent Wiener processes. Since we assume the global coupling, one can rewrite the model (4) as

$$dx_i = [f(x_i) + K(X - x_i)] dt + \alpha dW_i(t), \quad (5)$$

where X is the mean field,

$$X := \frac{1}{N} \sum_{j=1}^N x_j. \quad (6)$$

Mean escape time

This research investigates the system's escape from $x = 0$ to $x = 1$, focusing on the mean escape time. We initialize the system to the lower state ($x = 0$) and analyze the time it takes for the system to escape to the upper one ($x = 1$). Technically, the first escape time of node i is defined as

$$\tau_i := \inf_t \{t > 0 \text{ such that } x_i(t) \geq \xi \text{ given } x_i(0) = 0\}, \quad (7)$$

where ξ is a fixed threshold between the lower and upper states. The value of ξ is arbitrary as long as it is not close to r or 1. We chose $\xi = 0.5$ in the following, but our results remain valid for other ξ values. As τ_i is defined for each node, we also define the average escape time,

$$\langle \tau_i \rangle := \frac{1}{N} \sum_{i=1}^N \tau_i. \quad (8)$$

The average $\langle \cdot \rangle$ is over nodes, not noise realizations. In other words, $\langle \tau_i \rangle$ is defined for each sample path. By taking expectation, we obtain the expected average escape time

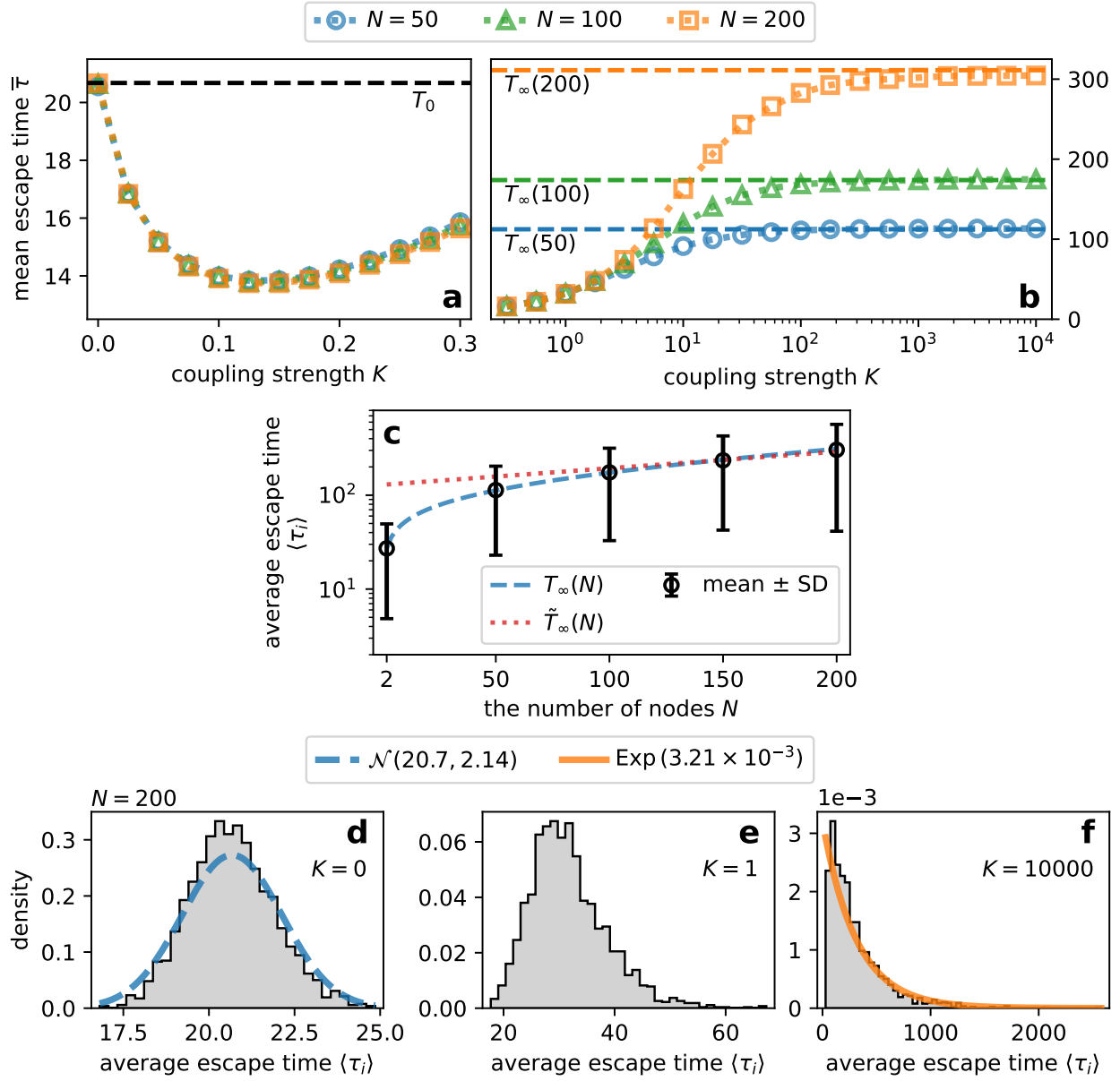
$$\bar{\tau} := \mathbb{E}[\langle \tau_i \rangle], \quad (9)$$

which we call mean escape time in this article. When the system is one dimensional, one can employ the following formula for mean escape time T [Section 5.5 in Ref.²⁸]:

$$T(\alpha) = \frac{2}{\alpha^2} \int_0^\xi dy \exp\left(\frac{V(y)}{\alpha^2/2}\right) \int_{-\infty}^y dz \exp\left(-\frac{V(z)}{\alpha^2/2}\right). \quad (10)$$

In addition to equation (10), Kramers' theory^{29,30} is often employed to study noise-induced escape²⁴⁻²⁶. The Kramers' formula for the mean escape time is the approximation of the formula (10) in the weak noise limit, and expressed as

$$\tilde{T}(\alpha) = \frac{2\pi}{\sqrt{V'''(0)|V'''(r)|}} \exp\left(\frac{V(r) - V(0)}{\alpha^2/2}\right). \quad (11)$$



[parameters] $r = 0.05$, $\alpha = 0.1$, $\xi = 0.5$, $dt = 2 \times 10^{-5}$, $\Delta t = 10^{-3}$, $n_{\text{trial}} = 2000$

Figure 2. The direct numerical simulations of the model [equation (5)] indicated that weak coupling reduced the mean escape time, while strong coupling impeded escape. (a, b) Numerically obtained mean escape time $\bar{\tau}$ against the coupling strength K for $N = 50, 100$, and 200 . (c) The system size dependence of average escape time $\langle \tau_i \rangle$ in the strong coupling limit. Black markers show the mean escape time $\bar{\tau}$, and error bars indicate standard deviations (SD). The blue dashed line is the prediction of equation (14), whereas the red dotted line indicates Kramers' formula [equation (15)]. (d – f) Histogram of average escape times for $K = 0, 1$ and 10000 . The dashed and solid lines show the theoretical probability distribution functions of the normal $[\mathcal{N}(T_0, T_0^2/N)]$ and exponential $[\text{Exp}(1/T_\infty(N))]$ distributions.

Results

Numerically measured mean escape time

Figures 2(a, b) plot the mean escape time against the coupling strength for $N = 50, 100,$ and 200 . The mean escape time was measured by direct numerical simulations of the model SDE (5). The figures exhibit the similar trends to the literature on a small system²³. That is, while weak coupling accelerated noise-induced escape, strong coupling impeded escape.

There are two trivial limiting cases. First, when there is no interaction, i.e. $K = 0$, all nodes are independent of each other. In this case, one expects the mean escape time to be

$$T_0 := T(\alpha), \quad (12)$$

which does not depend on the system size N . Figure 2(a) shows the mean escape time at $K = 0$ indeed coincided with T_0 for all N . Second, in the limit of strong coupling, i.e. $K \rightarrow \infty$, differences among nodes' states decay so fast that one may assume $x_i \approx X$. The system reduces to the following one-dimensional system for the mean field X :

$$dX = f(X) dt + \frac{\alpha}{\sqrt{N}} dW_X(t), \quad (13)$$

where $W_X(t)$ is a standard Wiener process. As the system is one-dimensional, one can employ the formulae for the mean escape time [equations (10) and (11)] with the reduced noise intensity α/\sqrt{N} :

$$T_\infty(N) := T\left(\alpha/\sqrt{N}\right), \quad (14)$$

$$\tilde{T}_\infty(N) := \tilde{T}\left(\alpha/\sqrt{N}\right). \quad (15)$$

Indeed, figure 2(b) demonstrates that the mean escape time saturated to approach $T_\infty(N)$ as K increased. In addition, the prediction of equation (14) was validated in figure 2(c). Figure 2(c) also shows Kramers' formula became relevant as N increased. This is because Kramers' formula is valid in the weak noise limit. We give more explanations on the two limiting cases in "Escape time in the two limiting cases" in Methods section.

Weak coupling facilitates escape

Figure 2(a) revealed weak coupling reduced the mean escape time with the minimum around $K \approx 0.15$. Since the coupling in our model is diffusive, it brings about the synchronization of nodes' states. That is, the stronger the coupling is, the more aligned each node's state is to the mean field. Therefore the coupling impedes escape when the mean field is small ($X \approx 0$), and it facilitates escape when X is large. When the coupling is very weak, the latter facilitating effect is dominant, which is why weak coupling reduced the mean escape time. In this subsection, we elaborate on the influence of weak coupling over noise-induced escape.

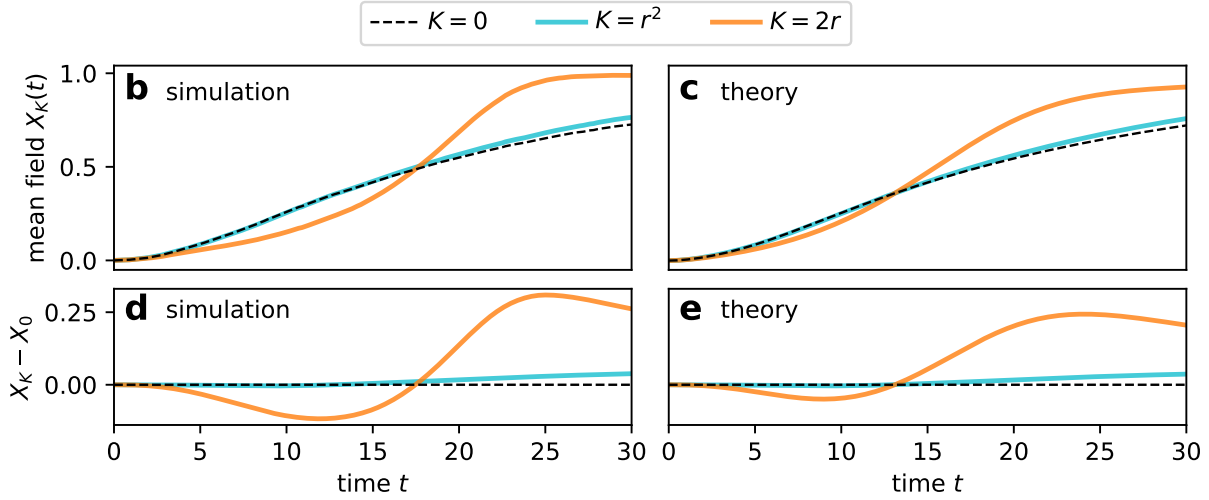
Figure 3(a) presents the temporal evolution of the mean field for several K values. The trajectories were obtained by numerical integration of the model SDE (5). One sees the mean field X monotonically increased, because we assumed r was so small that we could neglect escape from the upper ($x = 1$) to lower ($x = 0$) state. This implies that the impeding effect would be dominant in the early period when X is small, and the facilitating effect would occur later.

To elucidate how weak coupling affects noise-induced escape, we focus on a node that has not yet escaped. In particular, we assume the order of the node's state x is $O(r)$ [figure 3(a)]. In this case, the leading term of $f(x)$ is $O(r^2)$, i.e. $f(x) \sim r^2$. When coupling is weak enough to satisfy $K \sim r^2$, the term $-Kx \sim r^3$ is negligible compared with the isolated dynamics $f(x)$. Moreover, when the mean field X is small enough to satisfy $X \sim r$, we have $KX \sim r^3$, implying that the whole coupling term $K(X-x)$ is negligible with regard to $f(x)$. After some time, the mean field X grows to be $O(1)$. Then, whereas the term $-Kx \sim r^3$ is still negligible, $KX \sim r^2$ becomes comparable to $f(x)$. The coupling term reduces as $K(X-x) \simeq KX > 0$, indicating that the coupling's dominant effect on escape is facilitating. In the case of $K \sim r$, i.e. less weak coupling, the $-Kx$ term is no longer negligible because $-Kx \sim r^2 \sim f(x)$. Furthermore, in the initial period where $X \sim r^2$, one may ignore $KX \sim r^3$ to obtain the effective coupling term of $K(X-x) \simeq -Kx$, which would be negative on average and thus impede escape.

Our argument is summarized in figure 3(a). When coupling is sufficiently weak to satisfy $K \sim r^2$, we expect (i) the dynamics are almost the same as that in the no coupling case ($K = 0$) in the early period, and (ii) only the facilitating effect occurs after the growth of the mean field. When the coupling strength is increased to become $K \sim r$, we also expect (iii) coupling impedes escape in the initial period. These expectation were confirmed in figures 3(b, d). First, the trajectories for $K = 0$ and r^2 overlap until around $t \approx 15$. Indeed, the difference between X_K for $K = r^2$ and X_0 [figure 3(d)] remained close to 0 in the early period. Second, the difference $X_K - X_0$ increased after the early period. The increase in the difference corresponds to the faster growth of X_K than X_0 , illustrating coupling's facilitating effect. Third, comparing the cases of $K = 0$ and $2r$, one finds that the growth of X_K was slower than X_0 in the early period, which demonstrates coupling's impeding effect.

a effect of diffusive coupling on noise-induced escape

x	K	X	drift	coupling's effect
$\mathcal{O}(r)$	$\mathcal{O}(r^2)$	$\mathcal{O}(r)$	$-rx + x^2 + \mathcal{O}(r^3)$	negligible
		$\mathcal{O}(1)$	$-rx + x^2 + KX + \mathcal{O}(r^3)$	facilitating
	$\mathcal{O}(r)$	$\mathcal{O}(r^2)$	$-rx + x^2 - Kx + \mathcal{O}(r^3)$	impeding
		$\mathcal{O}(r)$	$-rx + x^2 + K(X - x) + \mathcal{O}(r^3)$	impeding & facilitating



[parameters] $r = 0.1$, $\alpha = 0.1$, $a = -0.5$, $b = 1.4$, $\Delta x = 10^{-3}$

Figure 3. The facilitating effect of diffusive coupling is dominant when coupling is sufficiently weak. (a) The leading terms of the drift term of the model SDE (5). Coupling may facilitate and impede noise-induced escape depending on the order of coupling strength K and the mean field value X . $x = \mathcal{O}(r)$ is assumed because we are interested in nodes that have not escaped. (b, c) Trajectories of $X_K(t)$, the mean field when the coupling strength is K . (d, e) The difference of $X_K(t)$ from $X_0(t)$ as a function of time. Panels (b) and (d) are the results of direct numerical simulations of the model SDE. Coupling was so weak that nodes were almost independent of each other. The trajectories of the mean field are thus nearly independent of noise realizations. Panels (c) and (e) are the results of our approximate theory.

To obtain quantitative insights into the mean escape time in weak coupling cases, we developed an approximate theory. Our arguments above imply that the initial evolution of the mean field is close to that in the uncoupled case when coupling is weak. We thus assume $X(t) \approx X_0(t)$, where $X_0(t)$ is the trajectory of the mean field when $K = 0$. Substituting $X_0(t)$ for X in the model SDE (5), our model becomes a one-dimensional system for x with the time-dependent parameter $X_0(t)$, for which one can solve the Fokker-Planck equation (FPE). The trajectory of $X_0(t)$ is also available by solving the FPE for the uncoupled model (1). Hence, by simultaneously solving the FPEs for uncoupled and weakly coupled models, we obtain the probability density function $p(t, x)$ for x at time t in weak coupling cases. One can furthermore compute the probability density function for escape times from $p(t, x)$. We refer readers to ‘‘Approximate theory for weak coupling cases’’ in Methods section for details.

Figures 3(c, e) present the estimated trajectories of the mean field $X_K(t)$ computed by our approximate theory. Comparing with the results from the direct numerical simulations [figures 3(b, d)], trajectories for $K = 0$ and r^2 seem almost identical, and the theoretical curves in figures 3(c, e) deviated from those in figures 3(b, d) for $K = 2r$. The difference between the actual $X(t)$ and $X_0(t)$, which is neglected in our theory, is naturally the cause of the deviation for $K = 2r$. Figure 4 shows the snapshots of the probability density functions. The upper peak around $x = 1$ at $t = 45$ was higher for stronger coupling, indicating the acceleration of the collective escape process. At $t = 10$ and 20 , one finds two peaks around $x = 0$ and 1 for $K = 0$ [figure 4(a)] and r^2 [figure 4(b)], but the distribution was no longer bimodal for $K = 2r$ [figure 4(c)]. This demonstrates the synchronizing effect of diffusive coupling. Figure 5 presents our main results for weak coupling cases, where the estimate from our theory is compared with the results of direct numerical simulations. By solving FPEs, one obtains not only the mean but also the

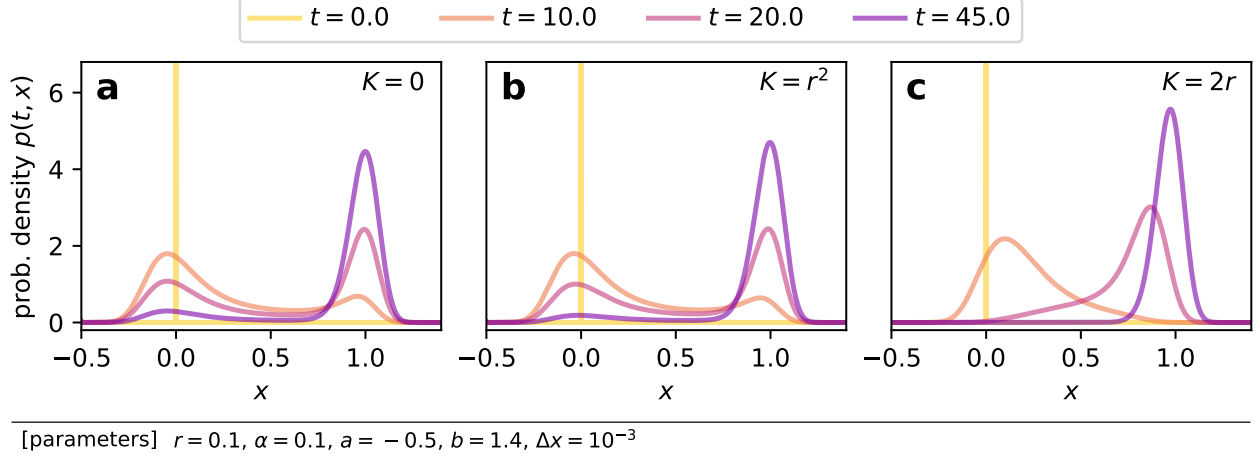


Figure 4. Evolution of the probability density function $p(t, x)$ according to our approximate Fokker-Planck equation (34).

variance of escape times τ_i , which are depicted by the dotted line and the area plot. Our estimates agreed surprisingly well to the simulation results as long as coupling was weak.

Strong coupling reduces the effective noise intensity

One sees from figures 2(a, b) that the mean escape time approached to the asymptotic value which was close to $T_\infty(N)$. We manually determined the asymptotic value, which is denoted by $\hat{\tau}_N$, and computed the difference of the mean escape time from $\hat{\tau}_N$. The result is presented in figure 6(a), where the difference $\hat{\tau}_N - \bar{\tau}$ is plotted against the coupling strength K . The figure illustrates that the difference scaled as K^{-1} when K was large. We argue that this is because the effective noise strength is reduced as K^{-1} as the coupling gets stronger.

To analyze the case of the finite coupling strength, i.e. $K \in (0, \infty)$, we introduce

$$y_i := x_i - X, \quad (16)$$

which is the displacement of node i from the mean field X . Neglecting higher order terms $O(y_i^2)$, the following equations describe the dynamics of X and y_i ,

$$dX = f(X) dt + \frac{\alpha}{\sqrt{N}} dW_X(t), \quad (17)$$

$$dy_i = -[K - f'(X)]y_i dt + \alpha \sqrt{\frac{N-1}{N}} d\tilde{W}_i(t), \quad i \in \{1, \dots, N-1\}, \quad (18)$$

where W_X and \tilde{W}_i are independent standard Wiener processes. Their derivations are in ‘‘Changing variables to the mean field and displacements’’ in Methods section. Unless K is so small that $f'(X) \geq K$, equation (18) describes the Ornstein-Uhlenbeck process whose mean is zero. When N is large and $K \gg f'(X)$, the variance of y_i would be approximately

$$\text{Var}[y_i] \simeq \frac{\alpha^2}{2K} \quad (19)$$

after a short $[O(K^{-1})]$ transient period. Equation (19) implies that, the stronger the coupling is, the closer the nodes are to the mean field X . In other words, strong coupling enhances synchronization among nodes, reducing the effective degree of freedom of the system. The results of numerical simulations shown in figure 6(b) illustrate the decline in the standard deviation of y_i as K increased, verifying equation (19).

Remembering $x_i = X + y_i$, equations (17) and (18) imply that x_i is always subjected to noise whose intensity is α/\sqrt{N} regardless of the coupling strength. This originates from the mean field dynamics [equation (17)]. The second term y_i is the Ornstein-Uhlenbeck process whose mean is 0 and variance is about $\alpha^2/(2K)$. Therefore we expect the effective noise intensity for x_i to be approximately

$$\sqrt{\frac{\alpha^2}{N} + c' \frac{\alpha^2}{2K}} \simeq \frac{\alpha}{\sqrt{N}} \left(1 + \frac{c}{K}\right) \quad (20)$$

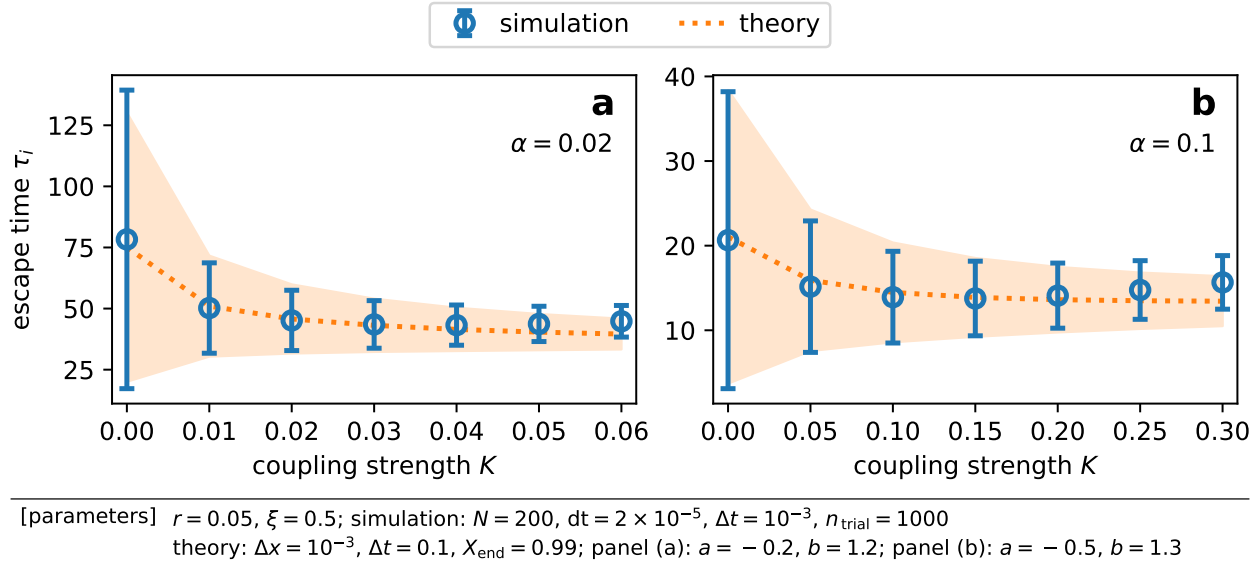


Figure 5. Our theory succeeded in estimating the mean and variance of escape times for different parameter values. (a, b) Comparison of the mean and standard deviation (SD) of escape times between direct simulations and our theory. Markers and error bars show respectively the mean escape time and the SD of escape times among nodes obtained through direct simulations. The dotted line and the filled area respectively indicate the mean and SD predicted by our theory.

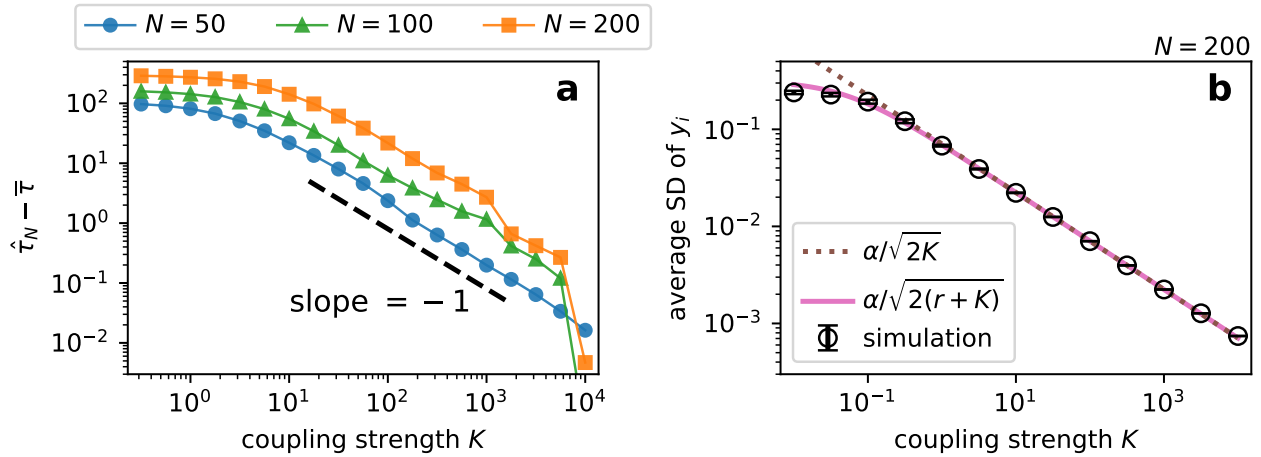
for large N and K , where c is some constant. This is why the difference $\hat{\tau}_N - \bar{\tau}$ scaled as K^{-1} . Indeed, if one fixes the value of c and substitutes equation (20) into equation (10), one obtains a similar curve to the ones shown in figure 6(a). We note however that we have not been able to systematically determine the coefficient c . This task is challenging, mainly because one must perform some kind of white approximation of the Ornstein-Uhlenbeck process y_i in order to derive the form $dx = \dots + \alpha/\sqrt{N}(1 + c/K) dW_{\text{effective}}(t)$.

Discussion

We studied the effect of the coupling strength on noise-induced escape for a system of globally coupled bistable elements. We numerically measured the mean escape time to observe that weak coupling reduced the mean escape time, whereas stronger coupling impeded escape [figures 2(a, b)]. We explained how weak coupling accelerates escape on average. Although diffusive coupling both facilitates and impedes escape, only the facilitating effect is dominant when coupling is weak, resulting in the decline in the mean escape time (figure 3). Based on this idea, we succeeded in estimating the mean and variance of escape times in weak coupling cases (figure 5). Finally, we reported that the difference of the mean escape time from its asymptotic value at $K \rightarrow \infty$ scaled as K^{-1} [figure 6(a)], which is due to the reduction in the effective noise intensity.

The phenomenon that weak coupling accelerates and strong coupling impedes noise-induced escape was reported for a two-node system in as early as 1982²³. Our results revealed their observations could be extended to larger systems. We furthermore gave an intuitive explanation for the way in which diffusive coupling affects the process of noise-induced escape. Coupling enables escaped nodes to pull others out from the lower state to facilitate escape, but at the same time allows nodes that have not escaped to gather around the lower state to impede escape. In addition, stronger coupling reduces the effective noise intensity. When coupling is sufficiently weak, the first facilitating effect is dominant. As coupling gets stronger, the second impeding effect becomes no longer negligible, and the balance between the facilitating and impeding effects determines the mean escape time. Under stronger coupling, all nodes fluctuate around the mean field, and the reduction in the effective noise intensity leads to the slow escape.

This research assumed that interaction among elements was diffusive. Another popular choice is additive coupling, which assumes each element is affected by the sum of its neighbors' states. Since additive and diffusive coupling can lead to different dynamics, the appropriate form of coupling must be determined when constructing a model⁶. Nonetheless diffusive coupling is of relevance to diverse topics. Diffusive coupling is a reasonable assumption when interaction involves flow of substances or individuals such as plants and animals. Among neurons, gap junction³¹ corresponds to diffusive coupling. We also believe diffusive coupling can describe social interaction among persons. Diverse states and behavior of human individuals, such as smoking³² and emotions³³, are known to spread through influence of peers, which is termed social contagion³⁴. Social learning



[parameters] $r = 0.05$, $\alpha = 0.1$, $\xi = 0.5$, $dt = 2 \times 10^{-5}$, $\Delta t = 10^{-3}$

panel (a): $n_{\text{trial}} = 2000$, $\hat{\tau}_{50} = 113.365$, $\hat{\tau}_{100} = 174.776$, $\hat{\tau}_{200} = 304.57$; panel (b): $n_{\text{trial}} = 100$, $t \in [0, 10]$

Figure 6. Strong coupling reduces the effective noise intensity, resulting in slow escape. (a) The difference of the numerically measured mean escape time $\bar{\tau}$ from the asymptotic value $\hat{\tau}_N$. (b) The average standard deviation (SD) of displacements y_i during $t \in [0, 10]$. The variance $\text{Var}[y_i] \approx \alpha^2/[2(K - f'(X))]$ is approximately $\alpha^2/[2(K+r)]$ when $X \ll 1$, which is shown by the solid line. When $r \ll K$, we obtain equation (19), which is indicated by the dotted line. The markers and error bars represent the mean and standard deviation of the simulation results.

through imitation^{35–37} is a salient mechanism by which behavior of an individual is affected by others. When an individual imitates those who are less similar, the magnitude of change in the person’s state would be greater. This illustrates resemblance between social interaction through imitation and diffusive coupling. We note, even if additive coupling is assumed in our model, weak coupling would still reduce the mean escape time. The additive coupling term under global coupling is $K/N \sum_j x_j = KX$, which is generally positive and thus facilitates escape.

In addition to diffusive coupling, this study assumed the asymmetric bistability, where the upper state is much more stable than the lower one. Nevertheless the effect of the coupling strength on the mean escape time would be qualitatively similar to our results when the potential is symmetric. That is, weak coupling would facilitate noise-induced escape, and strong coupling would reduce the effective noise intensity to impede escape. The symmetric case is especially relevant in studying stochastic resonance³⁸. When the coupling strength is fixed to a large value, one would observe stochastic resonance by changing the system size, as the effective noise intensity is about α/\sqrt{N} . Indeed, such phenomena is known as system size resonance³⁹. Moreover, since the transition rate changes according to the coupling strength, one also observes stochastic resonance by changing the coupling strength, instead of the noise intensity. This coupling-induced stochastic resonance may allow for the empirical estimation of the coupling strength. For instance, one may conduct stochastic resonance experiments for a system of interacting elements⁴⁰ and its isolated element. Because weak (strong, respectively) coupling increases (reduces) the transition rate, one expects the interaction within the system to be weak (strong) if the optimal noise intensity for the whole system is smaller (larger) than that for an isolated element.

Our results suggest that the diffusive coupling among multistable elements contributes to regulating the transition rate among attracting states. When each element is subjected to noise, interaction with others changes the rate of noise-induced escape. Strong coupling would be appropriate for a system where the high stability of a particular attracting state is favorable, since it reduces the transition rate. In contrast, weak coupling can improve the efficiency of some process by facilitating escape. It is particularly interesting if weak coupling promotes stochastic resonance that is unattainable without the coupling. Putting it another way, when the environmental noise is too weak to induce stochastic resonance, weak coupling may amplify the effective noise to achieve the optimum noise intensity for resonance. Previous studies have argued that stochastic resonance enhances sensory capacities^{41,42}. Our results indicate the possibility that relevant systems, perhaps neuronal systems, evolved to have weak coupling among their components so that they can exploit stochastic resonance.

We restricted ourselves to studying the expected average escape time, which we referred to as the mean escape time. Depending on the context, other quantities may well be used to characterize the escape process of the whole system. Our results would be qualitatively valid even if one adopts different quantities such as the expected escape time of the last node $\mathbb{E}[\tau_N]$ and the expected median of escape times. However, it is no longer the case if one focuses on the expected escape time of nodes that

escape early, for instance $\mathbb{E}[\tau_1]$. Indeed, the expected escape time of the first node $\mathbb{E}[\tau_1]$, also known as extreme first passage time⁴³, would monotonically increase as the diffusive coupling becomes stronger, because the coupling reduces the variance in escape times among nodes.

While this research is limited to the global coupling case, the influence of the coupling strength over the mean escape time would be qualitatively similar for other network structures. For general network cases, it might be possible to perform similar analyses to ours by introducing the mean field weighted by nodes' degrees, instead of the simple mean field X . Another interesting direction for future research is the introduction of heterogeneity. In various real systems, the shape of the potential determined by r is likely to differ across elements. The coupling strength may also vary across interactions, i.e. across edges in a network. Our work lays the foundation for such research on noise-induced escape in a heterogeneous system.

Methods

Changing variables to the mean field and displacements

In this subsection, we rewrite the system (5) in terms of mean field X and displacements $y_i := x_i - X$. From equations (5) and (6), one can write

$$\frac{dX}{dt} = \frac{1}{N} \sum_{j=1}^N f(X+y_j) + \frac{\alpha}{N} \sum_{j=1}^N \eta_j, \quad (21)$$

$$\frac{dy_i}{dt} = f(X+y_i) - \frac{1}{N} \sum_{j=1}^N f(X+y_j) - Ky_i + \frac{\alpha}{N} \left[(N-1)\eta_i - \sum_{j \neq i} \eta_j \right], \quad i \in \{1, \dots, N-1\} \quad (22)$$

where η_i are independent white gaussian noise with zero mean and unit variance.

In the drift terms in equations (21) and (22), we expand $f(X+y)$ as

$$f(X+y) = f(X) + f'(X)y + \mathcal{O}(y^2) \quad (23)$$

and neglect $\mathcal{O}(y^2)$ to obtain

$$\frac{1}{N} \sum_{j=1}^N f(X+y_j) \simeq f(X), \quad (24)$$

$$f(X+y_i) - \frac{1}{N} \sum_{j=1}^N f(X+y_j) \simeq f'(X)y_i. \quad (25)$$

As for the noise terms, from the reproductive property of gaussian distribution, one can rewrite the terms as

$$\frac{\alpha}{N} \sum_{j=1}^N \eta_j = \frac{\alpha}{\sqrt{N}} \eta_X, \quad (26)$$

$$\frac{\alpha}{N} \left[(N-1)\eta_i - \sum_{j \neq i} \eta_j \right] = \alpha \sqrt{\frac{N-1}{N}} \tilde{\eta}_i, \quad (27)$$

where η_X and $\tilde{\eta}_i$ independently follow $\mathcal{N}(0, 1)$. The variables (x_i) and (X, y_i) has the following relation,

$$\begin{pmatrix} X \\ y_1 \\ \vdots \\ y_{N-1} \end{pmatrix} = \frac{1}{N} \begin{pmatrix} 1 & 1 & \cdots & 1 \\ N-1 & -1 & \cdots & -1 \\ \vdots & \ddots & \ddots & \vdots \\ -1 & \cdots & N-1 & -1 \end{pmatrix} \begin{pmatrix} x_1 \\ x_2 \\ \vdots \\ x_N \end{pmatrix}. \quad (28)$$

Since the inner product of the first and subsequent rows of the matrix equals to zero, X and y_i , and similarly η_X and $\tilde{\eta}_i$, are independent. Putting equations (24, 25, 26, 27) into equations (21) and (22), we obtain

$$\frac{dX}{dt} = f(X) + \frac{\alpha}{\sqrt{N}} \eta_X, \quad (29)$$

$$\frac{dy_i}{dt} = -[K - f'(X)]y_i + \alpha \sqrt{\frac{N-1}{N}} \tilde{\eta}_i, \quad i \in \{1, \dots, N-1\}, \quad (30)$$

i.e. equations (17) and (18).

Escape time in the two limiting cases

When there is no interaction, i.e. $K = 0$, τ_i are independent samples from the distribution for escape times, which has an exponential tail in the weak noise limit^{26,30}. Thus $\langle \tau_i \rangle$ is a sample average of τ_i that are independently sampled from the asymptotic exponential distribution, whose mean is T_0 [equation (12)]. The variance of the exponential distribution is T_0^2 . Furthermore, since the mean escape time $\bar{\tau}$ is the average of sample averages, $\langle \tau_i \rangle$ would follow a normal distribution with mean T_0 and variance T_0^2/N due to the central limit theorem, if the sample size N is large enough. This expectation was confirmed in figure 2(d).

In the case of infinitely strong coupling, $K \rightarrow \infty$, since the system is effectively one-dimensional, the average escape time would follow an exponential distribution whose mean is $T_\infty(N)$ [equation (14)] in the limit of $K \rightarrow \infty$. As expected, the numerically obtained distribution of average escape times had an exponential tail [figure 2(f)].

Approximate theory for weak coupling cases

The Fokker-Planck equation (FPE) for the uncoupled model (1) is

$$\frac{\partial p_0(t,x)}{\partial t} = -\frac{\partial}{\partial x} [f(x)p_0(t,x)] + \frac{\alpha^2}{2} \frac{\partial^2 p_0(t,x)}{\partial x^2}, \quad (31)$$

where $p_0(t,x)$ is the probability density function (PDF) for x at time t . Using $p_0(t,x)$, the mean field in the uncoupled case, $X_0(t)$, can be calculated as

$$X_0(t) = \int_{-\infty}^{\infty} x p_0(t,x) dx. \quad (32)$$

By replacing X with X_0 in the model SDE (5), the model becomes

$$dx = [f(x) + K(X_0(t) - x)] dt + \alpha dW(t), \quad (33)$$

whose FPE is

$$\frac{\partial p(t,x)}{\partial t} = -\frac{\partial}{\partial x} [f(x) - K(X_0(t) - x)] p(t,x) + \frac{\alpha^2}{2} \frac{\partial^2 p(t,x)}{\partial x^2} \quad (34)$$

$$=: -\frac{\partial J(t,x)}{\partial x}, \quad (35)$$

where we defined the probability current $J(t,x)$. $J(t,x)$ represents the probability density that passes through x at time t . We expect the probability density mostly moves towards the upper state around $x = \xi$ because of the strong asymmetry of the potential, i.e. small r . Therefore we may regard $J(t,\xi)$ as the PDF for the escape time τ_i . That is, $J(t,\xi)$ is the probability that a node escapes at time t . Using $J(t,\xi)$, we can compute the mean and variance of escape times as follows:

$$\bar{\tau} = \mathbb{E}[\tau_i] = \int_0^{\infty} t J(t,\xi) dt, \quad (36)$$

$$\text{Var}[\tau_i] = \mathbb{E}[\tau_i^2] - (\bar{\tau})^2 = \int_0^{\infty} t^2 J(t,\xi) dt - (\bar{\tau})^2 \quad (37)$$

To obtain our results, we numerically solved FPEs (31) and (34) simultaneously to calculate the PDF $p(t,x)$, from which the probability current $J(t,x)$ was computed. We assumed both $p = 0$ and $\partial_x p = 0$ at the boundaries $x = a$ and b . We used the central difference to approximate the space derivative with step size Δx , obtaining a system of ordinary differential equations on discretized space. Integrals such as the ones in equations (32), (36), and (37) were approximated by summations within finite sections.

Numerical methods and parameters

Table 1 is the list of parameters that appear in this paper. We noted specific parameter values used to obtain the corresponding results in each figure so as to eliminate room for a mistake in transcribing values into the manuscript. For numerical integration of SDEs, we implemented the Euler-Maruyama method with fixed time step dt . The results were sampled with the time interval of Δt due to memory limitation. To obtain first escape times numerically, we simulated the model SDE [equation (5)] from the initial condition of $x_i = 0$ for all i . We say node i has escaped when $x_i \geq \xi$ holds for a given threshold ξ . Each simulation run was terminated when all nodes had escaped, and the first time step when $x_i \geq \xi$ was satisfied was recorded as τ_i for each node. For each parameter value, this process was repeated n_{trial} times, using different seeds for the random number generator. For numerical integration of ordinary differential equations, we used `scipy.integrate.solve_ivp()` method with Python. The parameters regarding the error tolerance, `a_tol` and `r_tol`, were both set to 10^{-8} . When solving the Fokker-Planck equations in our approximate theory, the results were sampled with the time interval of Δt due to memory limitation. This was done by assigning `t_eval` argument so that the solver interpolated values at $t = j \Delta t$ ($j \in \mathbb{N}$).

Table 1. A list of parameters that appear in this paper. Specific values of relevant parameters are indicated in each figure.

parameter	description
r	The location of the potential barrier.
α	The noise intensity.
N	The number of nodes.
K	The coupling strength.
ξ	The threshold to determine the escape time.
n_{trial}	The number of trials, i.e. sample paths.
dt	The step size in time used in the Euler-Maruyama method.
Δt	The time interval to sample results of numerical integration.
seed	The seed for a random number generator.
a	The lower end of the state space to solve Fokker-Planck equations.
b	The upper end of the state space to solve Fokker-Planck equations.
Δx	The step size in space to discretize space derivatives in Fokker-Planck equations.
X_{end}	Numerical integration of Fokker-Planck equations was terminated when the mean field X exceeded X_{end} .

Data Availability

The data and scripts used in this research are available in the GitHub repository, <https://github.com/ishihihidemasa/24-coupling-facilitate-impede-escape>.

References

- Kalitzin, S. N., Velis, D. N. & Lopes da Silva, F. H. Stimulation-based anticipation and control of state transitions in the epileptic brain. *Epilepsy & Behav.* **17**, 310–323, DOI: [10.1016/j.yebeh.2009.12.023](https://doi.org/10.1016/j.yebeh.2009.12.023) (2010).
- May, R. M. Thresholds and breakpoints in ecosystems with a multiplicity of stable states. *Nature* **269**, 471–477, DOI: [10.1038/269471a0](https://doi.org/10.1038/269471a0) (1977).
- Herbig, P. A. A cusp catastrophe model of the adoption of an industrial innovation. *J. Prod. Innov. Manag.* **8**, 127–137, DOI: [10.1016/0737-6782\(91\)90006-K](https://doi.org/10.1016/0737-6782(91)90006-K) (1991).
- May, R. M., Levin, S. A. & Sugihara, G. Ecology for bankers. *Nature* **451**, 893–894, DOI: [10.1038/451893a](https://doi.org/10.1038/451893a) (2008).
- Benjamin, O. *et al.* A phenomenological model of seizure initiation suggests network structure may explain seizure frequency in idiopathic generalised epilepsy. *The J. Math. Neurosci.* **2**, 1, DOI: [10.1186/2190-8567-2-1](https://doi.org/10.1186/2190-8567-2-1) (2012).
- Lopes, M. A., Hamandi, K., Zhang, J. & Creaser, J. L. The role of additive and diffusive coupling on the dynamics of neural populations. *Sci. Reports* **13**, 4115, DOI: [10.1038/s41598-023-30172-3](https://doi.org/10.1038/s41598-023-30172-3) (2023).
- Dakos, V., van Nes, E. H., Donangelo, R., Fort, H. & Scheffer, M. Spatial correlation as leading indicator of catastrophic shifts. *Theor. Ecol.* **3**, 163–174, DOI: [10.1007/s12080-009-0060-6](https://doi.org/10.1007/s12080-009-0060-6) (2010).
- Wunderling, N., Donges, J. F., Kurths, J. & Winkelmann, R. Interacting tipping elements increase risk of climate domino effects under global warming. *Earth Syst. Dyn.* **12**, 601–619, DOI: [10.5194/esd-12-601-2021](https://doi.org/10.5194/esd-12-601-2021) (2021).
- Barrett, C. B. & Swallow, B. M. Fractal poverty traps. *World Dev.* **34**, 1–15, DOI: [10.1016/j.worlddev.2005.06.008](https://doi.org/10.1016/j.worlddev.2005.06.008) (2006).
- Brummitt, C. D., Barnett, G. & D’Souza, R. M. Coupled catastrophes: Sudden shifts cascade and hop among interdependent systems. *J. The Royal Soc. Interface* **12**, 20150712, DOI: [10.1098/rsif.2015.0712](https://doi.org/10.1098/rsif.2015.0712) (2015).
- Krönke, J. *et al.* Dynamics of tipping cascades on complex networks. *Phys. Rev. E* **101**, 042311, DOI: [10.1103/PhysRevE.101.042311](https://doi.org/10.1103/PhysRevE.101.042311) (2020).
- Scheffer, M. *et al.* Early-warning signals for critical transitions. *Nature* **461**, 53–59, DOI: [10.1038/nature08227](https://doi.org/10.1038/nature08227) (2009).
- Kundu, P., MacLaren, N. G., Kori, H. & Masuda, N. Mean-field theory for double-well systems on degree-heterogeneous networks. *Proc. Royal Soc. A: Math. Phys. Eng. Sci.* **478**, 20220350, DOI: [10.1098/rspa.2022.0350](https://doi.org/10.1098/rspa.2022.0350) (2022).
- MacLaren, N. G., Kundu, P. & Masuda, N. Early warnings for multi-stage transitions in dynamics on networks. *J. The Royal Soc. Interface* **20**, 20220743, DOI: [10.1098/rsif.2022.0743](https://doi.org/10.1098/rsif.2022.0743) (2023).
- Booth, V. & Erneux, T. Mechanisms for propagation failure in discrete reaction-diffusion systems. *Phys. A: Stat. Mech. its Appl.* **188**, 206–209, DOI: [10.1016/0378-4371\(92\)90267-T](https://doi.org/10.1016/0378-4371(92)90267-T) (1992).

16. Erneux, T. & Nicolis, G. Propagating waves in discrete bistable reaction-diffusion systems. *Phys. D: Nonlinear Phenom.* **67**, 237–244, DOI: [10.1016/0167-2789\(93\)90208-I](https://doi.org/10.1016/0167-2789(93)90208-I) (1993).
17. Kouvaris, N. E., Kori, H. & Mikhailov, A. S. Traveling and Pinned Fronts in Bistable Reaction-Diffusion Systems on Networks. *PLOS ONE* **7**, e45029, DOI: [10.1371/journal.pone.0045029](https://doi.org/10.1371/journal.pone.0045029) (2012).
18. Caputo, J.-G., Cruz-Pacheco, G. & Panayotaros, P. Bistable reaction–diffusion on a network. *J. Phys. A: Math. Theor.* **48**, 075102, DOI: [10.1088/1751-8113/48/7/075102](https://doi.org/10.1088/1751-8113/48/7/075102) (2015).
19. Nadkarni, N., Arrieta, A. F., Chong, C., Kochmann, D. M. & Daraio, C. Unidirectional Transition Waves in Bistable Lattices. *Phys. Rev. Lett.* **116**, 244501, DOI: [10.1103/PhysRevLett.116.244501](https://doi.org/10.1103/PhysRevLett.116.244501) (2016).
20. Raney, J. R. *et al.* Stable propagation of mechanical signals in soft media using stored elastic energy. *Proc. Natl. Acad. Sci.* **113**, 9722–9727, DOI: [10.1073/pnas.1604838113](https://doi.org/10.1073/pnas.1604838113) (2016).
21. Kouvaris, N. E., Sebek, M., Mikhailov, A. S. & Kiss, I. Z. Self-Organized Stationary Patterns in Networks of Bistable Chemical Reactions. *Angewandte Chemie Int. Ed.* **55**, 13267–13270, DOI: [10.1002/anie.201607030](https://doi.org/10.1002/anie.201607030) (2016).
22. Kouvaris, N. E., Sebek, M., Iribarne, A., Díaz-Guilera, A. & Kiss, I. Z. Stationary patterns in star networks of bistable units: Theory and application to chemical reactions. *Phys. Rev. E* **95**, 042203, DOI: [10.1103/PhysRevE.95.042203](https://doi.org/10.1103/PhysRevE.95.042203) (2017).
23. Frankowicz, M. & Gudowska-Nowak, E. Stochastic simulation of a bistable chemical system: The two-box model. *Phys. A: Stat. Mech. its Appl.* **116**, 331–344, DOI: [10.1016/0378-4371\(82\)90249-7](https://doi.org/10.1016/0378-4371(82)90249-7) (1982).
24. Neiman, A. Synchronizationlike phenomena in coupled stochastic bistable systems. *Phys. Rev. E* **49**, 3484–3487, DOI: [10.1103/PhysRevE.49.3484](https://doi.org/10.1103/PhysRevE.49.3484) (1994).
25. Ashwin, P., Creaser, J. & Tsaneva-Atanasova, K. Fast and slow domino regimes in transient network dynamics. *Phys. Rev. E* **96**, 052309, DOI: [10.1103/PhysRevE.96.052309](https://doi.org/10.1103/PhysRevE.96.052309) (2017).
26. Creaser, J., Tsaneva-Atanasova, K. & Ashwin, P. Sequential Noise-Induced Escapes for Oscillatory Network Dynamics. *SIAM J. on Appl. Dyn. Syst.* **17**, 500–525, DOI: [10.1137/17M1126412](https://doi.org/10.1137/17M1126412) (2018).
27. Schlögl, F. Chemical reaction models for non-equilibrium phase transitions. *Zeitschrift für Physik* **253**, 147–161, DOI: [10.1007/BF01379769](https://doi.org/10.1007/BF01379769) (1972).
28. Gardiner, C. *Stochastic Methods*. Springer Series in Synergetics (Springer-Verlag, Berlin, Heidelberg, 2009), fourth edn.
29. Kramers, H. A. Brownian motion in a field of force and the diffusion model of chemical reactions. *Physica* **7**, 284–304, DOI: [10.1016/S0031-8914\(40\)90098-2](https://doi.org/10.1016/S0031-8914(40)90098-2) (1940).
30. Berglund, N. Kramers’ law: Validity, derivations and generalisations, DOI: [10.48550/arXiv.1106.5799](https://doi.org/10.48550/arXiv.1106.5799) (2013). [1106.5799](https://arxiv.org/abs/1106.5799).
31. Trenholm, S. & Awatramani, G. B. Myriad roles for gap junctions in retinal circuits. In Kolb, H., Fernandez, E. & Nelson, R. (eds.) *Webvision: The Organization of the Retina and Visual System [Internet]* (University of Utah Health Sciences Center, Salt Lake City (UT), 2019).
32. Ali, M. M. & Dwyer, D. S. Estimating Peer Effects in Adolescent Smoking Behavior: A Longitudinal Analysis. *J. Adolesc. Heal.* **45**, 402–408, DOI: [10.1016/j.jadohealth.2009.02.004](https://doi.org/10.1016/j.jadohealth.2009.02.004) (2009).
33. Kramer, A. D. I., Guillory, J. E. & Hancock, J. T. Experimental evidence of massive-scale emotional contagion through social networks. *Proc. Natl. Acad. Sci.* **111**, 8788–8790, DOI: [10.1073/pnas.1320040111](https://doi.org/10.1073/pnas.1320040111) (2014).
34. Christakis, N. A. & Fowler, J. H. Social contagion theory: Examining dynamic social networks and human behavior. *Stat. Medicine* **32**, 556–577, DOI: [10.1002/sim.5408](https://doi.org/10.1002/sim.5408) (2013).
35. Whiten, A., McGuigan, N., Marshall-Pescini, S. & Hopper, L. M. Emulation, imitation, over-imitation and the scope of culture for child and chimpanzee. *Philos. Transactions Royal Soc. B: Biol. Sci.* **364**, 2417–2428, DOI: [10.1098/rstb.2009.0069](https://doi.org/10.1098/rstb.2009.0069) (2009).
36. Chartrand, T. L. & Lakin, J. L. The Antecedents and Consequences of Human Behavioral Mimicry. *Annu. Rev. Psychol.* **64**, 285–308, DOI: [10.1146/annurev-psych-113011-143754](https://doi.org/10.1146/annurev-psych-113011-143754) (2013).
37. Tamura, K., Kobayashi, Y. & Ihara, Y. Evolution of individual versus social learning on social networks. *J. The Royal Soc. Interface* **12**, 20141285, DOI: [10.1098/rsif.2014.1285](https://doi.org/10.1098/rsif.2014.1285) (2015).
38. Gammaitoni, L., Hänggi, P., Jung, P. & Marchesoni, F. Stochastic resonance. *Rev. Mod. Phys.* **70**, 223–287, DOI: [10.1103/RevModPhys.70.223](https://doi.org/10.1103/RevModPhys.70.223) (1998).
39. Pikovsky, A., Zaikin, A. & de la Casa, M. A. System Size Resonance in Coupled Noisy Systems and in the Ising Model. *Phys. Rev. Lett.* **88**, 050601, DOI: [10.1103/PhysRevLett.88.050601](https://doi.org/10.1103/PhysRevLett.88.050601) (2002).

40. Gluckman, B. J. *et al.* Stochastic Resonance in a Neuronal Network from Mammalian Brain. *Phys. Rev. Lett.* **77**, 4098–4101, DOI: [10.1103/PhysRevLett.77.4098](https://doi.org/10.1103/PhysRevLett.77.4098) (1996).
41. Russell, D. F., Wilkens, L. A. & Moss, F. Use of behavioural stochastic resonance by paddle fish for feeding. *Nature* **402**, 291–294, DOI: [10.1038/46279](https://doi.org/10.1038/46279) (1999).
42. Itzcovich, E., Riani, M. & Sannita, W. G. Stochastic resonance improves vision in the severely impaired. *Sci. Reports* **7**, 12840, DOI: [10.1038/s41598-017-12906-2](https://doi.org/10.1038/s41598-017-12906-2) (2017).
43. Lawley, S. D. Distribution of extreme first passage times of diffusion. *J. Math. Biol.* **80**, 2301–2325, DOI: [10.1007/s00285-020-01496-9](https://doi.org/10.1007/s00285-020-01496-9) (2020).

Acknowledgements

We thank Istvan Z. Kiss, Hajime Koike, Naoki Masuda, and Yuzuru Sato for valuable comments. This study was supported by the World-leading Innovative Graduate Study Program in Proactive Environmental Studies (WINGS-PES), the University of Tokyo, to H.I., and JSPS KAKENHI (No. JP21K12056) to H.K.

Author contributions statement

H.I. and H.K. conceived this project. H.I. conducted numerical simulations, analyzed the results, and wrote the manuscript in consultation with H.K.

Additional information

Competing interests The authors declare no competing interests.